

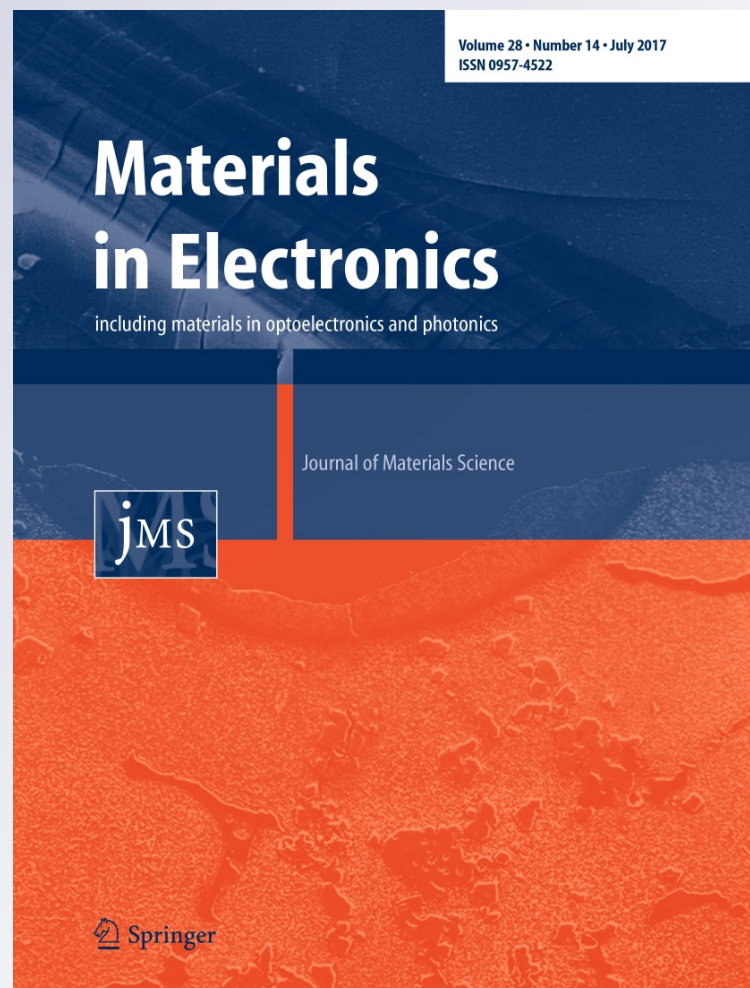
*Investigation of Cu–Sn–Se material
for high-speed phase-change memory
applications*

**Haipeng You, Yifeng Hu, Xiaoqin Zhu,
Hua Zou, Sannian Song & Zhitang Song**

**Journal of Materials Science:
Materials in Electronics**

ISSN 0957-4522
Volume 28
Number 14

J Mater Sci: Mater Electron (2017)
28:10199-10204
DOI 10.1007/s10854-017-6784-y



Your article is protected by copyright and all rights are held exclusively by Springer Science +Business Media New York. This e-offprint is for personal use only and shall not be self-archived in electronic repositories. If you wish to self-archive your article, please use the accepted manuscript version for posting on your own website. You may further deposit the accepted manuscript version in any repository, provided it is only made publicly available 12 months after official publication or later and provided acknowledgement is given to the original source of publication and a link is inserted to the published article on Springer's website. The link must be accompanied by the following text: "The final publication is available at link.springer.com".

Investigation of Cu–Sn–Se material for high-speed phase-change memory applications

Haipeng You¹ · Yifeng Hu¹ · Xiaoqin Zhu¹ · Hua Zou¹ · Sannian Song² · Zhitang Song²

Received: 24 February 2017 / Accepted: 16 March 2017 / Published online: 21 March 2017
© Springer Science+Business Media New York 2017

Abstract Cu–Sn–Se material was prepared by magnetron sputtering to investigate its potential application in phase change memory. The amorphous-to-crystalline transition was studied by in situ film resistance measurements. Cu–Sn–Se material had lower activation energy for crystallization (1.60 eV) and higher crystallization resistance than SnSe. The amorphous Cu–Sn–Se had more narrow band gap compared to SnSe. After the adding of Cu, the crystallization of Cu–Sn–Se material was inhibited and the grain structure became more compact. The picosecond laser pulse measurement indicated that Cu–Sn–Se material had a fast phase change speed (3.36 ns). The results demonstrated that Cu–Sn–Se material was a promising phase change material which had low power and high speed application in phase change memory.

1 Introduction

Nowadays with the rapid development of non-volatile memory (NVM), there is no doubt that phase change memory (PCM) has been regarded as one of the best candidates for the next-generation memory which has some advantages such as fast switching speed, high scalability and low

power [1–3]. Meanwhile, not only does phase change memory have good data retention, but also it has fabrication compatibility with complementary metal–oxide–semiconductor (CMOS) process [4, 5]. The stocked data is gained by optical switching between the amorphous and crystalline states. The data stored can be also recovered by means of utilizing variation of the reflectivity optically between crystalline and amorphous states [6, 7].

As we all know, it is Ge₂Sb₂Te₅ (GST) that is currently the extensively adopted phase change material, which has shown outstanding performance [8]. However, GST has some shortcomings in some aspects. It, for example, is difficult for the GST-based PCM devices to have integrated SET and RESET processes when the electric pulse width is shorter than 100 ns [9]. Additionally, GST material also has poor thermal stability (85 °C for 10 years) because Te atoms in GST materials can easily segregate to the interfaces between phase change material and heating electrode on account of their high mobility and low melting temperature [10, 11]. Recently, there are some materials which have been indicated to have fast crystallization rate and good amorphous thermal stability like GeTe [12], SnSb [13] and ZnSb [14]. Besides, the doping has been applied to improve the thermal property of phase change materials effectively [15].

In the work, it is Cu-doped SnSe material that is recommended and detailedly introduced by resistance versus temperature (R – T), scanning electronic microscopy (SEM) and surface topography measurements. The effect of Cu-doping on the thermal stability, crystallization characteristics and optical transition of Cu–SnSe phase-change material are analyzed.

✉ Yifeng Hu
hyf@jsut.edu.cn

✉ Xiaoqin Zhu
pcram@jsut.edu.cn

¹ School of Mathematics and Physics, Jiangsu University of Technology, Changzhou 213000, China

² State Key Laboratory of Functional Materials for Informatics, Shanghai Institute of Micro-System and Information Technology, Chinese Academy of Sciences, Shanghai 200050, China

2 Experiment

The experiment process was divided into two parts. The first part mainly talked about the manufacture process of two kinds of thin film. Prior to the sputtering coating, SiO₂ substrate should be put on the sample plate through double-sided adhesive. Also, magnetron sputtering apparatus needs to be vacuum. The pressure of magnetron sputtering apparatus was 4×10^{-4} pa before sputtering. Then, Cu-doped and un-doped Sn₄₆Se₅₄ thin films were deposited on SiO₂ substrates when the pressure of sputtering was 4×10^{-1} pa. The total gas flow of Ar was fixed at 30 sccm (sccm denotes standard cubic centimeter per minute at STP). Finally, Cu-doped thin film was achieved under Ar sputtering gas. The SnSe and CuSnSe films represented undoped and Cu-doped SnSe films, respectively.

The second part described about how to examine properties and structure of SnSe and CuSnSe films. The transition from amorphous to crystalline was researched by in situ temperature dependent conductivity and resistance measurement. The sample temperature was measured by a Pt-100 thermocouple located at a heating stage controlled by a TP 94 temperature controller (Linkam Scientific Instruments Ltd, Surrey, UK). The purity of SnSe and Cu targets were 99.999% and thin films thickness was set to 50 nm by the means of controlling the deposition time. The optical band gap was measured by NIR spectrophotometer. The phase structures of the films which were annealed at various temperatures were investigated by XRD analyses using Cu K α radiation in the 2θ range from 20° to 60°, with a scanning step of 0.01°. Roughness on the surface of the material could be examined by atomic force microscopy (AFM, FM-Nanoview 1000). The grain states of phase change materials before and after the crystallization were observed by scanning electron microscopy (SEM, Hitachi S-4700). A picosecond laser pump–probe system was used for real-time reflectivity measurement. The light source used for irradiating the samples was a frequency-doubled model-locked neodymium yttrium aluminum garnet laser operating at 532 nm wave-length a pulse duration of 30 ps. The chemical compositions of Sn, Se and Cu element in SnSe and CuSnSe thin films, determined by the energy dispersive X-ray analysis (Oxford INCA Energy), were around 46, 54 and 28, 33, 39 at.%, respectively.

3 Result and discussion

Figure 1 exhibits the change in the resistance as a function of the heating temperature at a constant rate of 30 °C/min for Sn₄₆Se₅₄, Cu₂₈Sn₃₃Se₃₉ and GST materials. As we can see, three materials are all in their high resistance states incipiently. Subsequently, a resistance drop dramatically

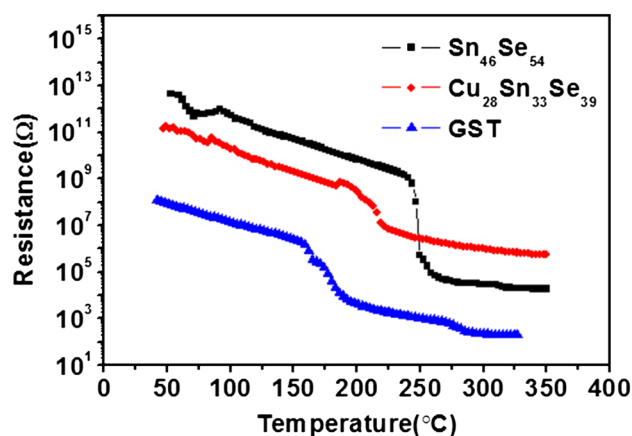


Fig. 1 Resistance of Sn₄₆Se₅₄, Cu₂₈Sn₃₃Se₃₉ and GST materials as a function of temperature at a heating rate of 30 °C/min

happens when the temperature reaches to a certain value which is seemed as the crystallization temperature T_c . Then, the resistance of all materials decreases slowly after T_c due to semiconductor-like effect. Figure 1 shows that the T_c for Sn₄₆Se₅₄, Cu₂₈Sn₃₃Se₃₉ and GST materials are 245, 195 and 165 °C. As is known to all, the thermal stability can be evaluated by the crystallization temperature roughly [16]. Thus, the thermal stability of Cu₂₈Sn₃₃Se₃₉ material is better than GST. Meanwhile, the crystallization resistance of Cu₂₈Sn₃₃Se₃₉ material is higher than Sn₄₆Se₅₄ material. According to the joule heat: $Q = I^2 R t$, where Q , I , R , and t are the thermal energy, current, electrical resistance, and time, respectively, a higher crystallization resistance can improve the heating efficiency and decrease the power consumption in RESET operation process [17]. Besides, the resistance difference for Cu₂₈Sn₃₃Se₃₉ before and after crystallization is more than two orders of magnitude which is enough for PCM applications.

The diffuse reflectivity spectra of Sn₄₆Se₅₄ and Cu₂₈Sn₃₃Se₃₉ materials are measured by NIR UV–visible–NIR spectrophotometry in the wavelength range from 400 to 2500 nm at room temperature. As is shown in Fig. 2, the band gap energy (E_g) can be determined by extrapolating the absorption edge onto the energy axis. Wherein the conversion of the reflectivity to absorbance data was obtained by the Kubelka–Munk function (K–M):

$$K/S = (1 - R)^2 / (2R) \quad (1)$$

where R , K and S are the reflectivity, absorption coefficient and scattering coefficient, respectively [18]. From Fig. 2, it shows the band gap energy for Sn₄₆Se₅₄ and Cu₂₈Sn₃₃Se₃₉ materials are 1.64 and 1.54 eV respectively, which indicates that Cu₂₈Sn₃₃Se₃₉ material has a smaller E_g than Sn₄₆Se₅₄ material. The dependent temperature for the resistivity in a semiconductor can be explained according to $\rho = \rho_0 \exp$

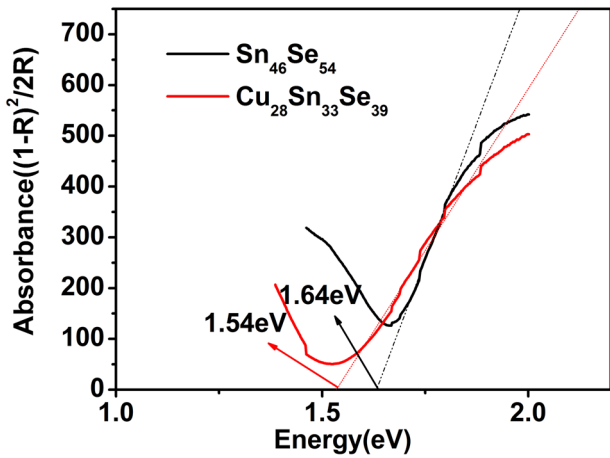


Fig. 2 The Kubelka–Munk function of amorphous Sn₄₆Se₅₄ and Cu₂₈Sn₃₃Se₃₉ materials

($-E_{\sigma}/kT$), where ρ is conductivity, ρ_0 is a pre-exponential factor and E_{σ} is the activation energy for electrical conduction. The activation energy of electrical transport is simply measured by half of the band gap $E_{\sigma} = E_g/2 + \Delta E$, where $E_g/2$ is the distance from the Fermi level to the conduction band and ΔE is depth of the trap states [19]. A decrease in the band gap will lead to the increase of carriers, which make a major contribution to the decreasing of film resistivity. Therefore, this finding can explain the change trends of resistance curves for Sn₄₆Se₅₄ and Cu₂₈Sn₃₃Se₃₉ materials in Fig. 1.

The activation energy for crystallization E_a is an important indicator to assess the difficulty for the crystallization. In order to obtain the E_a , the resistance versus temperature curves with different heating rates of 10, 20, 30 and 40 °C/min are conducted (not shown here). With a faster heating rate, phase change material will have a higher crystallization temperature T_c because it does not have enough time to accumulate the energy for crystallization. The E_a of Sn₄₆Se₅₄ and Cu₂₈Sn₃₃Se₃₉ materials can be calculated from a Kissinger equation:

$$\left[\frac{dT}{dt} / T_c^2 \right] = C + E_a / (k_b T_c) \quad (2)$$

where dT/dt is the heating rate, T_c is the crystallization temperature, C is a constant, E_a is the activation energy for crystallization and k_b is Boltzmann's constant [20]. From the slope of the linear fit in the $\ln[(dT/dt)/T_c^2]$ versus $1/T_c$ curves in Fig. 3, the value of E_a for Sn₄₆Se₅₄ and Cu₂₈Sn₃₃Se₃₉ materials are 3.79 and 1.60 eV, respectively. It is obvious that the E_a of Cu-doped Sn₄₆Se₅₄ material decreases. A lower E_a implies lower energy barrier for crystallization, which will result in a shorter SET time for the PCM cells. From this point, Cu₂₈Sn₃₃Se₃₉ material has a faster switching speed than Sn₄₆Se₅₄, which is very significant in practical application.

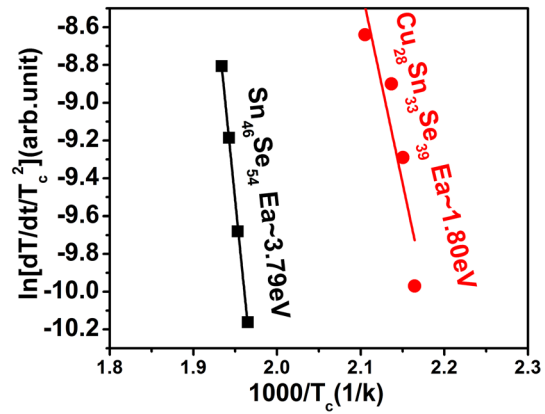


Fig. 3 The Kissinger plots $\ln[(dT/dt)/T_c^2]$ versus $1/(KT_c)$ of Sn₄₆Se₅₄ and Cu₂₈Sn₃₃Se₃₉ materials

The XRD patterns of Sn₄₆Se₅₄ and Cu₂₈Sn₃₃Se₃₉ materials annealed at different temperatures are shown in Fig. 4a, b, respectively. For Sn₄₆Se₅₄ and Cu₂₈Sn₃₃Se₃₉ materials, there are no clear diffraction peak in the as-deposited samples indicating an amorphous structure. With the increasing

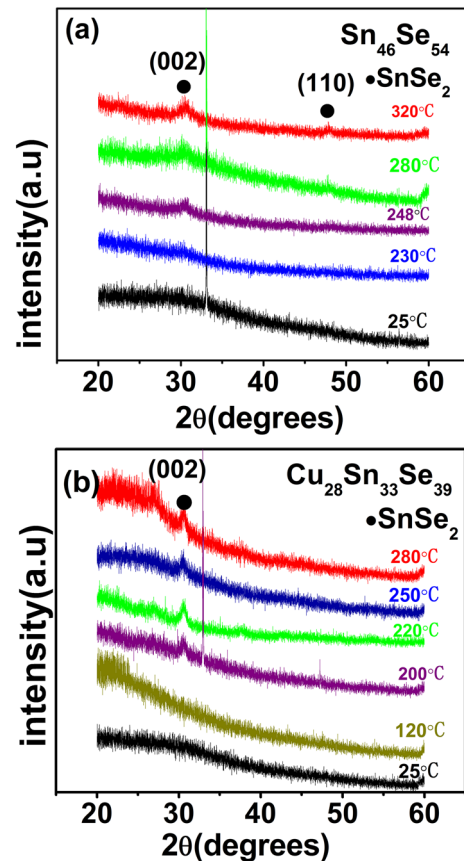


Fig. 4 XRD patterns of **a** Sn₄₆Se₅₄, **b** Cu₂₈Sn₃₃Se₃₉ materials annealed at different temperatures for 10 min in Ar atmosphere

of annealing temperature, the first appearance of diffraction peak (002) is at the temperature 200 °C for $\text{Cu}_{28}\text{Sn}_{33}\text{Se}_{39}$ material in Fig. 4b. Being different from $\text{Cu}_{28}\text{Sn}_{33}\text{Se}_{39}$, no diffraction peaks are observed at the temperature 230 °C for $\text{Sn}_{46}\text{Se}_{54}$. It manifests that $\text{Sn}_{46}\text{Se}_{54}$ has better amorphous thermal stability than $\text{Cu}_{28}\text{Sn}_{33}\text{Se}_{39}$ material, which is in accord with the result of Fig. 1. Subsequently, a characteristic peak (110) belonging to $\text{Sn}_{46}\text{Se}_{54}$ phase appears for $\text{Sn}_{46}\text{Se}_{54}$ after annealing at 248 °C for 10 min in the Fig. 4. Then, a new diffraction peak (110) is observed in 280 and 320 °C annealed $\text{Sn}_{46}\text{Se}_{54}$ material, indicating the crystallization strengthened further. For $\text{Cu}_{28}\text{Sn}_{33}\text{Se}_{39}$, there is no other diffraction peak except SnSe_2 (002), indicating the crystallization has been restrained by Cu adding. From the main peak at around 30.5° with the same annealing temperature 280 °C, the grain sizes of annealed $\text{Sn}_{46}\text{Se}_{54}$ and $\text{Cu}_{28}\text{Sn}_{33}\text{Se}_{39}$ materials are 7.60 and 4.77 nm, respectively, which are calculated using the Scherrer ($D_{hkl} = 0.943\lambda/\beta\cos\theta$) [21]. The decreased grain size can produce more grain boundaries, which will help to enhance the electron scattering, leading to a higher resistance. This result interprets the resistance increasing of $\text{Cu}_{28}\text{Sn}_{33}\text{Se}_{39}$ material compared with $\text{Sn}_{46}\text{Se}_{54}$ on the structural aspect.

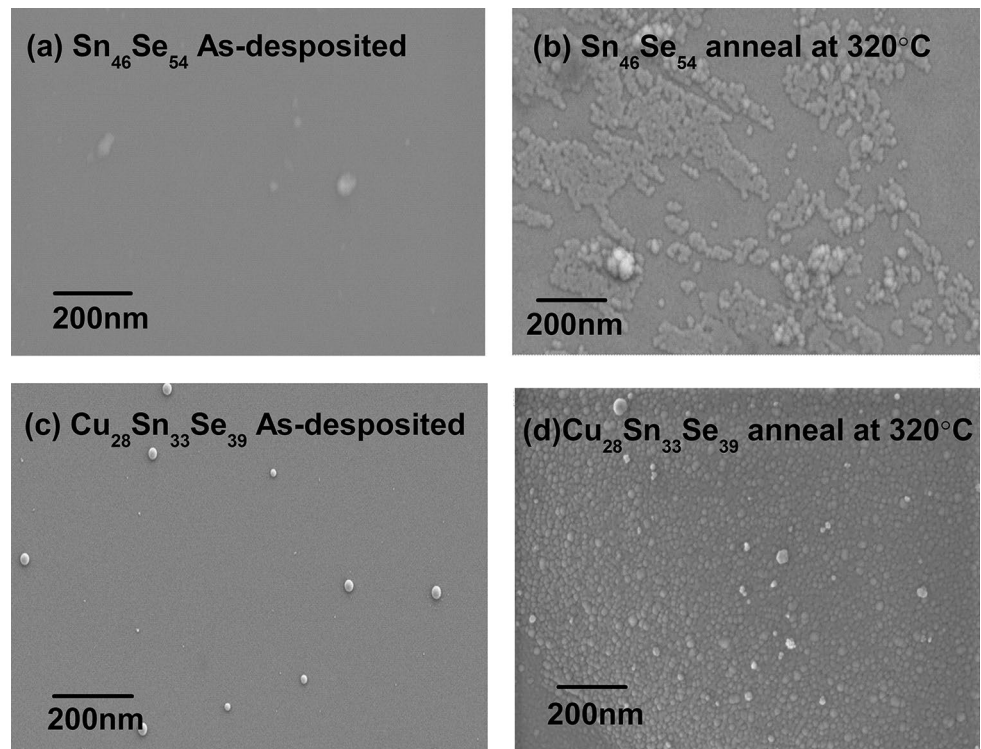
The SEM surface images of as-deposit and annealed $\text{Sn}_{46}\text{Se}_{54}$ and $\text{Cu}_{28}\text{Sn}_{33}\text{Se}_{39}$ materials are shown in Fig. 5a–d, respectively. Figure 5a shows no obvious grains which are seen in as-deposited $\text{Sn}_{46}\text{Se}_{54}$ material. Meanwhile, as we can see in Fig. 5c, a few grains have formed for $\text{Cu}_{28}\text{Sn}_{33}\text{Se}_{39}$. From this point, it indicates that

$\text{Cu}_{28}\text{Sn}_{33}\text{Se}_{39}$ material is easier to crystallize because of its lower activation energy for crystallization compared with $\text{Sn}_{46}\text{Se}_{54}$ material. After annealing at 320 °C for 10 min, more grains for $\text{Sn}_{46}\text{Se}_{54}$ and $\text{Cu}_{28}\text{Sn}_{33}\text{Se}_{39}$ form in Fig. 5b, d. Numerous grains for $\text{Cu}_{28}\text{Sn}_{33}\text{Se}_{39}$ material are assigned to a mixture of orthorhombic and hexagonal phases. From Fig. 5b, it shows sparse grains for $\text{Sn}_{46}\text{Se}_{54}$ material. However, the grains are more compact for annealed $\text{Cu}_{28}\text{Sn}_{33}\text{Se}_{39}$. Therefore, more grain boundaries exist in $\text{Cu}_{28}\text{Sn}_{33}\text{Se}_{39}$, which corresponds with the XRD pattern in Fig. 4 [22].

Figure 6 presents the AFM images of $\text{Sn}_{46}\text{Se}_{54}$ and $\text{Cu}_{28}\text{Sn}_{33}\text{Se}_{39}$ materials before and after crystallization. As is known, the internal stress of materials will result in the change of surface in phase change process. For PCM, the surface roughness of any materials has an important impact on device performance because it will affect the quality of the electrode-film interface [23]. The surface of as-deposited $\text{Sn}_{46}\text{Se}_{54}$ and $\text{Cu}_{28}\text{Sn}_{33}\text{Se}_{39}$ materials are smooth, with the root-mean-square surface roughness 0.5479 and 1.1458 nm for $\text{Sn}_{46}\text{Se}_{54}$ and $\text{Cu}_{28}\text{Sn}_{33}\text{Se}_{39}$, respectively. After annealing at 320 °C for 10 min, the roughness of $\text{Sn}_{46}\text{Se}_{54}$ and $\text{Cu}_{28}\text{Sn}_{33}\text{Se}_{39}$ material increases to 0.4881 and 1.6334 nm. It is this result that implies that the internal stress of $\text{Cu}_{28}\text{Sn}_{33}\text{Se}_{39}$ is comparatively small, which can assure the endurance of PCM devices.

In the phase switching process, the dramatic change of resistivity is accompanied by the optical reflectivity. The evolution of reflectivity during amorphization and

Fig. 5 SEM images of as-deposited and annealed $\text{Sn}_{46}\text{Se}_{54}$ and $\text{Cu}_{28}\text{Sn}_{33}\text{Se}_{39}$ materials



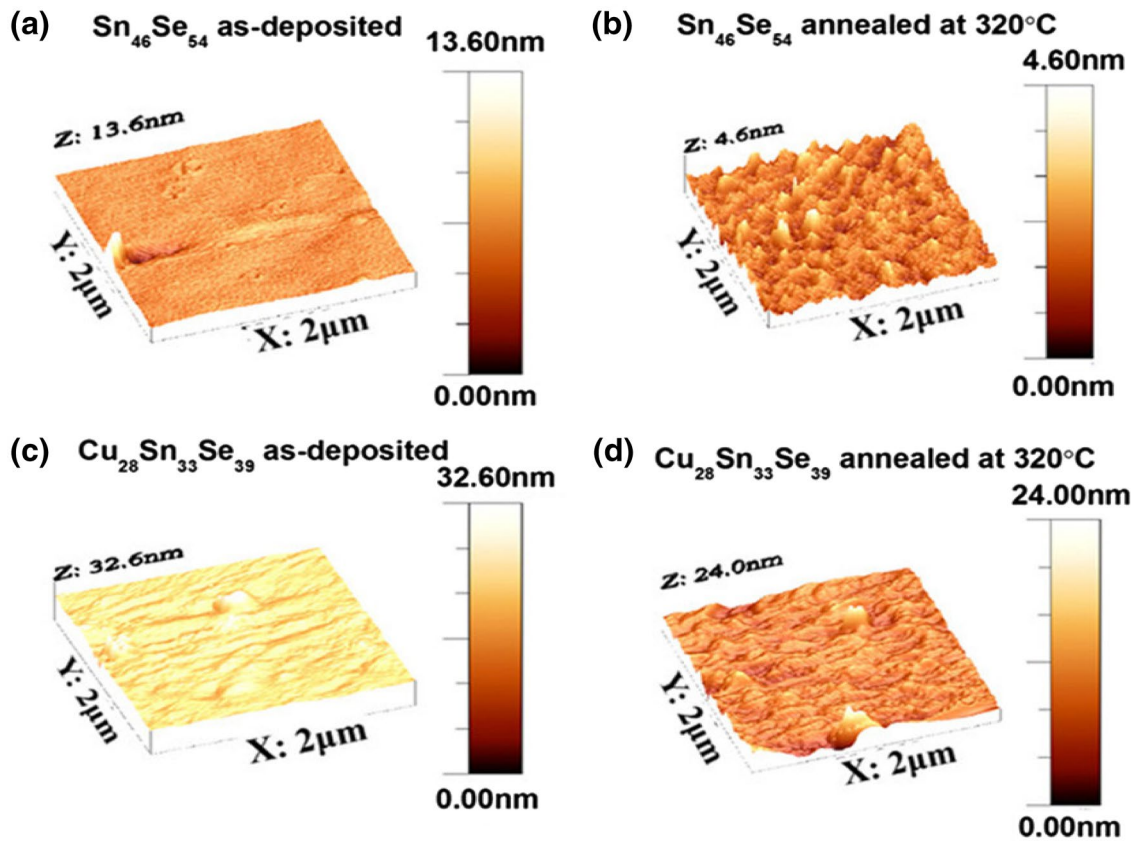


Fig. 6 AFM topographic images of **a** as-deposited $\text{Sn}_{46}\text{Se}_{54}$, **b** annealed $\text{Sn}_{46}\text{Se}_{54}$ at 320°C , **c** as-deposited $\text{Cu}_{28}\text{Sn}_{33}\text{Se}_{39}$, **d** annealed $\text{Cu}_{28}\text{Sn}_{33}\text{Se}_{39}$ at 320°C

crystallization processes are measured by the picosecond pulse laser, which is intended to study the phase change speed. As shown in Fig. 7a, the reflectivity of all curves maintains a high value until a sudden drop which corresponds the crystalline-to-amorphous state transition. The time of amorphization process are 5.71, 4.61 and 3.62 ns, with the irradiation fluences of 16.5, 19.2 and 20.3 mJ/cm^2 , respectively. It is a shorter switching time that can be obtained in a higher irradiation fluence. Then, the converse phase changes are accomplished with a dramatic increase of optical reflectivity in Fig. 7b. The process of crystallization needs more time than amorphization process, so the crystallization time is used to be the standard value of phase-change speed. Then crystallization times are 4.41, 3.86 and 3.36 ns when the irradiation fluences are 2.65, 2.78 and 3.56 mJ/cm^2 , respectively. As is known to all, it is the crystallization time of GST that is 39 ns, which is induced by a laser irradiation fluence of 11.59 mJ/cm^2 [24]. Therefore, the switching speed of $\text{Cu}_{28}\text{Sn}_{33}\text{Se}_{39}$ material is much faster than GST.

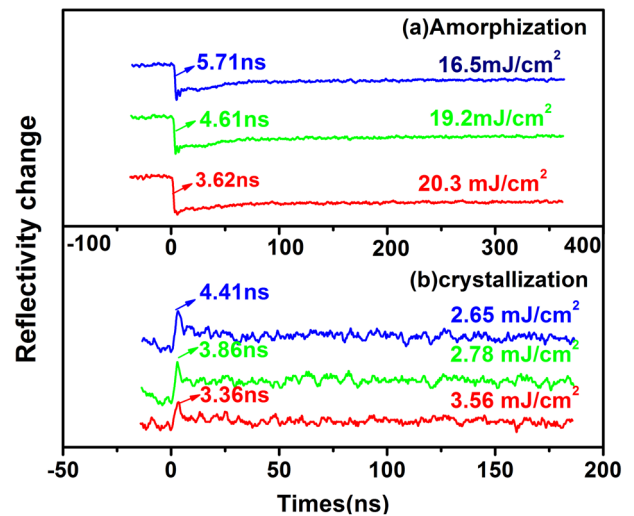


Fig. 7 Reversible reflectivity evolution of $\text{Cu}_{28}\text{Sn}_{33}\text{Se}_{39}$ material induced by consecutive picosecond laser pulses with different fluences: (a) amorphization process (b) crystallization process

4 Conclusion

Compared with $\text{Sn}_{46}\text{Se}_{54}$ material, $\text{Cu}_{28}\text{Sn}_{33}\text{Se}_{39}$ has a lower activation energy for crystallization (1.60 eV) and a higher crystallization state resistance. The energy band gap of amorphous $\text{Cu}_{28}\text{Sn}_{33}\text{Se}_{39}$ becomes more narrow after Cu doping, which leads to the increase of the carrier concentration and the decrease of SET operation power. Besides, the adding of Cu inhibits the crystallization $\text{Sn}_{46}\text{Se}_{54}$ material, resulting smaller grain size of $\text{Cu}_{28}\text{Sn}_{33}\text{Se}_{39}$ (4.77 nm) and more compact grain structure. A good surface roughness of 1.1458 nm measured by AFM for crystalline $\text{Cu}_{28}\text{Sn}_{33}\text{Se}_{39}$ can ensure the quality of the electrode–film interface. The picosecond pulse laser measurement demonstrates that the $\text{Cu}_{28}\text{Sn}_{33}\text{Se}_{39}$ material has a fast crystallization speed of 3.36 ns. Therefore, $\text{Cu}_{28}\text{Sn}_{33}\text{Se}_{39}$ material is a promising candidate for its fast phase change speed in PCM application.

Acknowledgements This work was supported by Natural Science Foundation of Jiangsu Province (BK20151172) and Changzhou Science and Technology Bureau (CJ20160028 and CJ20159049) and Basic Research Program of Jiangsu Education Department (15KJB430012) and sponsored by Qing Lan Project.

References

1. Y.F. Hu, X.Q. Zhu, H. Zou, J.H. Zhang, L. Yuan, J.Z. Xue, Y.M. Sui, W.H. Wu, S.N. Song, Z.T. Song, *Appl. Phys. Lett.* **108**(22), 223103 (2016)
2. Y.F. Hu, M.C. Sun, S.N. Song, Z.T. Song, J.W. Zhai, *Integr. Ferroelectr.* **140**(1): 8–15 (2012).
3. M.C. Sun, Y.F. Hu, B. Shen, J.W. Zhai, S.N. Song, Z.T. Song, *Integr. Ferroelectr.* **140**(1): 1–7 (2012).
4. Y.F. Hu, Z.F. He, J.W. Zhai, P.Z. Wu, T.S. Lai, S.N. Song, Z.T. Song, *Appl. Phys. A* **121**(3): 1125–1131 (2015).
5. Y.F. Hu, S.M. Li, T.S. Lai, S.N. Song, Z.T. Song, J.W. Zhai, *J. Alloys Compd.* **581**, 515–518 (2013)
6. W. Zhang, D. Wu, Y.F. Hu, A.R. Jiang, J.S. Xu, H. Liu, S.P. Bu, R.H. Shi, *J. Mater. Sci. Mater. Electron.* **27**: 4908–4912 (2016).
7. W.H. Wu, Y.F. Hu, X.Q. Zhu, Y.M. Sui, J.Z. Xue, L. Yuan, S.N. Song, Z.T. Song, *J. Mater. Sci. Mater. Electron.* **26**: 9700–9706 (2015).
8. X.Q. Zhu, Y.F. Hu, H. Zou, J.H. Zhang, Y.M. Sun, W.H. Wu, L. Yuan, L.J. Zhai, S.N. Song, Z.T. Song, *Scr. Mater.* **121**, 66–69 (2016)
9. Y.G. Lu, S.N. S, X. Shen, Z.T. Song, L.C. Wu, G.X. Wang, and S.X. Dai, *Appl. Phys. A* **117**(4): 1933–1940 (2014).
10. H. Zou, X.S. Wang, Y.F. Hu, X.Q. Zhu, Y.M. Sui, D.H. Shen, Z.T. Song, *J. Mater. Sci. Mater. Electron.* **26**(9): 6502–6505 (2015).
11. F.F. Wei, L. Wang, T. Kong, L. Shi, R. Huang, J. Zhang, G.S. Chen, *Appl. Phys. Lett.* **103**(18), 181908 (2013)
12. H.Y. Cheng, S. Raoux, J.L. Jordan-Sweet, *Appl. Phys.* **115**(9), 093101 (2014)
13. Z.F. He, P.Z. Wu, R.R. Liu, J.W. Zhai, T.S. Lai, S.N. Song, Z.T. Song, *CrystEngComm* **18**(7), 1230–1234 (2016)
14. G.X. Wang, X. Shen, Y.G. Lu, S.X. Dai, Q.H. Nie, T.F. Xu, *J. Alloys Compd.* **622**, 341–346 (2015)
15. Y.G. Lu, S.N. Song, X. Shen, Z.T. Song, G.X. Wang, S.X. Dai, *Thin Solid Films* **589**, 215–220 (2015)
16. T. Morikawa, K. Kurotsuchi, Y. Fujisaki, Y. Matsui, N. Takaura, *Jpn. J. Appl. Phys.* **51**(3), 031201 (2012)
17. F. Wang, T. Zhang, C.L. Liu, Z.T. Song, L.C. Wu, B. Liu, S.L. Feng, B. Chen, *Appl. Surf. Sci.* **254**(8), 2281–2284 (2008)
18. M.-J. Xia, F. Rao, Z.-T. Song, K. Ren, L.-C. Wu, B. Liu, S.-L. Feng, *Phys. Lett.* **30**(3), 037401 (2013)
19. Y.G. Lu, M. Wang, S.N. Song, M.J. Xia, Y. Jia, X. Shen, G.X. Wang, S.X. Dai, Z.T. Song, *Appl. Phys. Lett.* **109**(17), 173103 (2016)
20. L. Jun-Tin, L. Yi-Bo, C. Meng-Hsueh, H. Wei-Chou, in 2009 IEEE International Conference on IC Design and Technology (ICICDT), 18–20 May 2009 (IEEE, Piscataway, 2009)
21. Y.G. Lu, S.M. Li, S.N. Song, Z.T. Song, B. Liu, T. Wen, T.S. Lai, 25650 North Lewis Way, Stevenson Ranch, California, 91381–1439, United States. American Scientific Publishers, 2013
22. F. Tong, X.S. Miao, Y. Wu, Z.P. Chen, H. Tong, X.M. Cheng, *Appl. Phys. Lett.* **97**(26), 261904 (2010)
23. C. Peng, L.C. Wu, Z.T. Song, X.L. Zhou, M. Zhu, F. Rao, B. Liu, S.L. Feng, *J. Non-Cryst. Solids* **358**(17), 2416–2419 (2012)
24. K. Ren, F. Rao, Z.T. Song, S.L. Lu, C. Peng, M. Zhu, L.C. Wu, B. Liu, S.L. Feng, *J. Alloys Compd.* **594**, 82–86 (2014)